Article

Cell Reports

A synthetic tear protein resolves dry eye through promoting corneal nerve regeneration

Graphical abstract

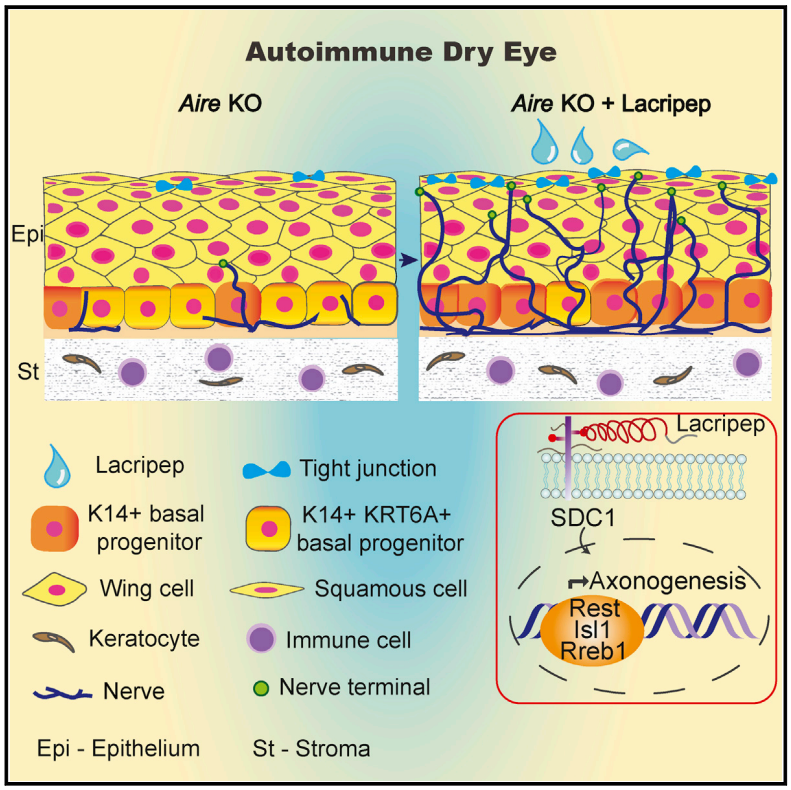

Highlights

- Lacripep promotes neuroregeneration in the desiccated cornea
- Lacripep rescues tearing, barrier function, homeostasis, and wound healing
- Aberrant basal epithelial cell identity is reversed by Lacripep treatment
- The regenerative actions of Lacripep occur despite extensive inflammation

Authors

Yael Efraim, Feeling Yu Ting Chen, Ka Neng Cheong, Eliza A. Gaylord, Nancy A. McNamara, Sarah M. Knox

Correspondence

nmcnamara@berkeley.edu (N.A.M.), sarah.knox@ucsf.edu (S.M.K.)

In brief

Currently, there are no regenerative treatments for ocular pathologies due to dry eye. Efraim et al. demonstrate the synthetic tear peptide Lacripep as a regenerative therapy capable of restoring the damaged, dysfunctional ocular surface to a near homeostatic state through promoting nerve regeneration in the presence of chronic inflammation.

Efraim et al., 2022, Cell Reports *40*, 111307
August 30, 2022
https://doi.org/10.1016/j.celrep.2022.111307

CellPress

Cell Reports

CellPress
OPEN ACCESS

Article

A synthetic tear protein resolves dry eye through promoting corneal nerve regeneration

Yael Efraim,[1,4] Feeling Yu Ting Chen,[1,4] Ka Neng Cheong,[1] Eliza A. Gaylord,[1] Nancy A. McNamara,[2,3,*] and Sarah M. Knox[1,5,*]

[1]Program in Craniofacial Biology, Department of Cell & Tissue Biology, University of California, San Francisco, San Francisco, CA 94143, USA
[2]Herbert Wertheim School of Optometry and Vision Science, University of California, Berkeley, Oakland, CA 94720, USA
[3]Department of Anatomy, University of California, San Francisco, San Francisco, CA 94143, USA
[4]These authors contributed equally
[5]Lead contact
*Correspondence: nmcnamara@berkeley.edu (N.A.M.), sarah.knox@ucsf.edu (S.M.K.)
https://doi.org/10.1016/j.celrep.2022.111307

SUMMARY

Corneal architecture is essential for vision and is greatly perturbed by the absence of tears due to the highly prevalent disorder dry eye. With no regenerative therapies available, pathological alterations of the ocular surface in response to dryness, including persistent epithelial defects and poor wound healing, result in life-long morbidity. Here, using a mouse model of aqueous-deficient dry eye, we reveal that topical application of the synthetic tear protein Lacripep reverses the pathological outcomes of dry eye through restoring the extensive network of corneal nerves that are essential for tear secretion, barrier function, epithelial homeostasis, and wound healing. Intriguingly, the restorative effects of Lacripep occur despite extensive immune cell infiltration, suggesting tissue reinnervation and regeneration can be achieved under chronic inflammatory conditions. In summary, our data highlight Lacripep as a first-in-class regenerative therapy for returning the cornea to a near homeostatic state in individuals who suffer from dry eye.

INTRODUCTION

Tear deficiency due to lacrimal gland dysfunction (aqueous-deficient dry eye) is among the most common and debilitating outcomes of systemic autoimmune diseases, including Sjögren syndrome, rheumatoid arthritis, scleroderma, and systemic lupus erythematosus (Lemp et al., 2007). A healthy tear film provides an aqueous coating necessary for optimal vision and tissue function while also shielding the ocular surface from environmental, inflammatory, and microbial insult. Due to the essential requirement of tears in maintaining ocular health, corruption of tissue integrity and loss of homeostasis in response to prolonged dryness induce a vast array of pathological outcomes (Pflugfelder et al., 2020). Yet, despite the extensive ramifications of dry eye on ocular health and its significant impact on vision, quality of life, and the psychological/physical consequences of chronic pain, there are currently only three clinically approved therapies for the treatment of dry eye disease that specifically target T cell-mediated inflammatory pathways believed to be the primary driver of dry eye pathogenesis. However, these anti-inflammatory treatments are not regenerative and only promote modest improvements in the signs and symptoms of dry eye (Pflugfelder et al., 2020), which results in life-long corneal dysfunction and reduced quality of life.

Due to the fundamental requirement for tears in corneal maintenance and the clear role of desiccating stress as a principal driver of dry eye pathogenesis, there has been a recent focus on the application of tear-promoting factors to relieve dry eye. Lacritin, an endogenous glycoprotein identified in tears that is deficient in patients with dry eye (Vijmasi et al., 2014), has been found to possess pro-secretory properties in healthy and diseased animal models (Samudre et al., 2011; Vijmasi et al., 2014), and to promote corneal epithelial cell proliferation *in vitro* (Wang et al., 2006). These findings led to the development of Lacripep, a stable synthetic peptide consisting of lacritin's active C-terminal fragment, which has also been shown to stabilize the human tear film (Georgiev et al., 2021). However, its impact on cornea regeneration, including tissue architecture and epithelial cell identity, integrity, and homeostasis, as well as physiological tear secretion, during dry eye disease progression has not been investigated. Furthermore, whether application of Lacripep to the desiccated cornea can restore the significantly depleted functional nerve supply that is essential for unstimulated (physiological) tear secretion, ocular surface integrity, and corneal wound healing/tissue regeneration, remains unknown.

Here, using the well-characterized, autoimmune regulator (*Aire*)-deficient mouse model of spontaneous, autoimmune-mediated dry eye, we show that topical administration of Lacripep resolves dry eye disease through reactivating physiological tear secretion, restoring progenitor cell identity, and rescuing epithelial barrier function. Lacripep achieves these outcomes through re-establishing functional sensory innervation of the corneal epithelium and can do so despite the presence of

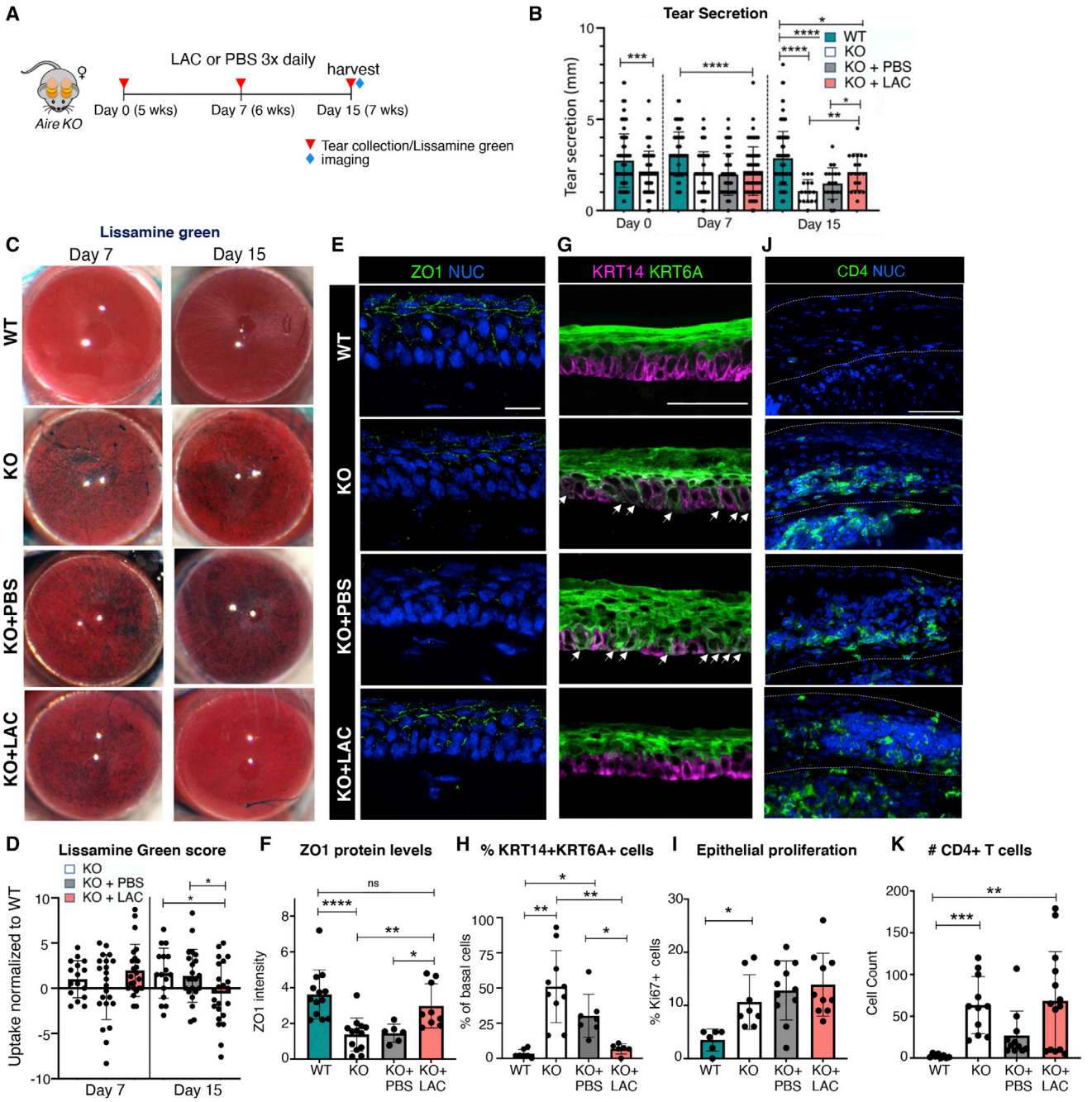

Figure 1. Physiological tear secretion, epithelial integrity, and basal progenitor cell identity are restored with Lacripep treatment during dry eye disease progression

(A) Schematic of treatment regimen showing data collection time points for tissue analysis.

(B) Levels of physiological (unstimulated) tear secretion at days 0, 7, and 15.

(C and D) Lissamine green uptake in untreated/treated *Aire* KO corneas compared with age-matched WT as assessed by scoring intensity of stain at days 7 and 15. The day 7 score was normalized to day 0 (before treatment) and the day 15 score was normalized to day 7. Data points above 1 indicate increased lissamine green uptake, while points below 1 indicate reduced uptake. NUC, nuclei.

(E–H) Immunofluorescent analysis and quantification of the tight junction protein ZO1 (E and F, scale bar, 20μm) and basal progenitor cell marker KRT14 and differentiation marker KRT6A (G and H, scale bar, 50μm) at day 15. Arrows in (G) highlight basal cells co-expressing KRT6A and KRT14. The graph in (H) shows the percentage of basal KRT14+ cells co-expressing KRT6A.

(I) Quantification of proliferating epithelial cells at day 15.

(legend continued on next page)

chronic ocular inflammation. Thus, we have identified a robust regenerative ocular therapeutic for dry eye disease that restores the secretory and epithelial integrity of the desiccated cornea through promoting sensory reinnervation.

RESULTS

Physiological tear secretion, epithelial integrity, and basal progenitor cell identity are restored with Lacripep treatment during dry eye disease progression

The process of tear secretion that occurs in response to changes at the ocular surface is essential to corneal function, homeostasis, and wound healing, and is profoundly reduced in human patients with dry eye disease. Although lacritin has been shown to promote physiological tear production (unstimulated) in a healthy rabbit model (Samudre et al., 2011), whether Lacripep is also capable of increasing tearing, and can do so during dry eye disease progression, is unknown. To test this, we evaluated tearing by utilizing the *Aire* mouse model of aqueous-deficient dry eye. *Aire* knockout (KO) female mice develop classic signs of dry eye disease over a 2-week time period. This begins with small lymphocytic infiltrates in the lacrimal glands and mildly reduced tear secretion, corneal innervation, and barrier function at 5 weeks (weeks), consistent with mild aqueous-deficient dry eye, that progresses to extensive CD4+ T cell-mediated exocrinopathy, severe reduction in stimulated tearing, and corneal pathologies at the epithelial, stromal, and nerve-associated levels by 7 weeks (Chen et al., 2017, 2018a; Efraim et al., 2020).

To determine the impact of Lacripep on tear secretion, Lacripep (4 μM) or phosphate-buffered saline (PBS) (control) was topically applied to *Aire* KO corneas three times (3×) per day for 14 consecutive days (from age 5 to 7 week) and tear production was measured at days 0, 7, and 15 (Figure 1A). Tear levels for the untreated *Aire* KO mice were significantly reduced at day 0 (77% of wild-type [WT] levels) and continued to decrease over time (67% at day 7 and 37% at day 15) (Figure 1B). Tearing was also significantly decreased for the PBS-treated mice, with tear volumes being 50% of the WT controls at day 15 (Figure 1B). Although Lacripep-treated *Aire* KO mice showed similar levels of tear production as untreated and PBS-treated mice at day 7, at day 15 tear volumes remained at day 0 levels (83% of WT) (Figure 1B), demonstrating that Lacripep retains pro-secretory functions during dry eye disease progression.

As dry eye results in disruption of ocular surface integrity resulting in cornea barrier dysfunction and, consequently, fluid loss and pathogen invasion, we next determined whether Lacripep maintains corneal epithelial architecture by analyzing lissamine green uptake at days 7 and 15. At day 7 all *Aire* KO treatment groups exhibited increased lissamine green uptake compared with WT controls (Figures 1C and 1D). However, at day 15, epithelial barrier function in Lacripep- but not PBS-treated or untreated corneas was significantly improved, with uptake levels resembling those of WT corneas (Figures 1C and 1D). Restoration of barrier function was further confirmed by analyzing the superficial epithelial layers for the tight junction protein ZO1, which is essential to the structural integrity of the corneal epithelium (Sugrue and Zieske, 1997). Levels of ZO1 were greatly reduced in the untreated and PBS-treated *Aire* KO cornea (Figures 1E and 1F). In contrast, ZO1 expression in Lacripep-treated corneas mimicked that of WT controls (Figures 1E and 1F); thus, demonstrating that Lacripep is sufficient to rescue functional integrity of the corneal epithelium.

Although it has been well established that basal progenitor cells (also referred to as transit amplifying cells; Di Girolamo et al., 2015) undergo mitosis and migration (Park et al., 2019) to give rise to the barrier forming suprabasal epithelial and stratified squamous epithelial cells, the impact of dry eye disease on basal cell identity and differentiation remains largely unknown. Thus, we questioned whether basal cell identity was altered in the desiccated cornea through defining the cellular location of KRT6A, a marker of early epithelial cell differentiation in skin (Boonekamp et al., 2019) and cultured cornea epithelial cells (Schermer et al., 1989). Accordingly, we confirmed that KRT6A marks differentiated corneal epithelial cell types *in vivo*, as shown by its exclusive expression in KRT14-deficient suprabasal and superficial epithelial cells of healthy corneas at age 7 weeks (Figure 1G). In contrast, KRT6A appeared in a large cohort of KRT14+ basal cells in the untreated *Aire* KO cornea (Figure 1G, arrows), suggesting that progenitors were undergoing aberrant differentiation. Treatment of *Aire* KO corneas with PBS for 2 weeks did not reverse this outcome, with the number of KRT6A+ KRT14+ cells being similar to untreated controls (Figures 1G and 1H). Strikingly, however, cell identity in Lacripep-treated corneas returned to that of WT tissue, with KRT6A remaining exclusively expressed by suprabasal/superficial cells (Figures 1G and 1H). To determine if changes in cell identity alter progenitor cell division, we analyzed the percentage of proliferating KRT14+ basal cells in treated and untreated corneas. In the untreated *Aire* KO corneas, KRT14+ cell division was significantly increased, as denoted by Ki67, compared with WT controls (Figure 1I). A similar outcome was found for both PBS- and Lacripep-treated *Aire* KO corneas, indicating that cell identity but not cell division is impacted by Lacripep.

We next tested whether Lacripep restored basal cell identity and barrier function by reducing immune cell infiltration. Prolonged desiccating stress from reduced tear production elicits an immune response in which activated CD4+ T cells home to the corneal epithelium and stroma (primarily accumulating at the limbal region) to modulate epithelial differentiation (Pflugfelder et al., 2008) and direct the development of autoimmune-mediated dry eye (Zhou et al., 2012). Intriguingly, at day 15 we found all *Aire* KO corneas (Figures 1I and 1J), as well as their corresponding lacrimal glands (Figures S1A and S1B), regardless of treatment, to be extensively infiltrated by CD4+ T cells.

(J–K) Immunofluorescent analysis and quantification of CD4+ T cells in WT and untreated/treated *Aire* KO corneas at day 15. Scale bar, 50 μm. *$p < 0.05$, **$p < 0.01$, ***$p < 0.001$, ****$p < 0.0001$; n.s., not significant. A one-way analysis of variance was applied to graphs (B, D, F, H, and K) with the following post-hoc tests: a Tukey's multiple comparisons test was used in (B, D, and F), and a Dunnett's T3 multiple comparisons test was used in (H and K). Graph (I) was analyzed using a one-way analysis of variance with correction for multiple comparisons using a false discovery rate of 0.05 and a two-stage step-up method of Benjamini, Krieger, and Yekutieli. Each dot in the bar graph represents a biological replicate. All data are expressed as mean + SD. n > 4 mice per group. See also Figure S1.

Furthermore, the extent of immune-mediated damage to *Aire* KO gland function under each condition was comparable as there was no difference between stimulated tear secretion in response to systemic injection of pilocarpine, a muscarinic agonist that directly activates muscarinic receptors on the lacrimal gland and goblet cells to stimulate tear production (Figure S1C). This outcome was further supported by RNA sequencing (RNA-seq) analysis at day 7 that showed (1) the expression of T cell markers, such as *Cd3*, *Cd7*, and *Cd8*, (2) T cell-specific response genes, such as T cell-specific guanine nucleotide triphosphate-binding protein 1 and 2 (*Tgtp1* and *Tgtp2*), and (3) macrophage markers, such as *Cd64*, remained significantly elevated in the untreated and PBS/Lacripep-treated *Aire* KO corneas compared with the WT controls (Figure S1D; Tables S1 and S2). In addition, key inflammatory mediators that are typically induced in desiccated corneas, including interleukin-1β (IL-1β), and interferon response genes (*Irgm1*, *Ifi203*, *Ifit1*, *Ccl22*, *Ccl5*, and *Stat1*) were expressed at similar levels in all diseased corneas (Figure S1D; Tables S1 and S2).

Thus, together these data indicate that, despite the ongoing, large-scale inflammatory response that occurs during dry eye disease progression, Lacripep is capable of improving corneal barrier function and rescuing cell identity in the desiccated cornea without dampening inflammation.

Sensory innervation of the desiccated cornea is restored in response to Lacripep treatment

As tear production is dependent on sensory innervation of the cornea, and dry eye leads to diminished corneal innervation in humans (Labbé et al., 2013; Li et al., 2021) and mice (Efraim et al., 2020; Simsek et al., 2018), we next determined whether the maintenance of tearing in response to Lacripep was due to restoration of the nerve supply. Sensory nerves derived from the ophthalmic lobe of the trigeminal ganglion primarily enter the corneal stroma at the limbal region and extend along the basement membrane, with axon fibers branching upward through the multi-layered epithelium to establish nerve-epithelial interactions. Here, they serve an essential role in sensing changes at the ocular surface (e.g., dryness) and maintaining corneal epithelial homeostasis, in part, through activation of tear production from the lacrimal gland via the lacrimal reflex. Thus, the degree of tearing reflects the function and quality of sensory nerves within the corneal epithelium. Consistent with this requirement, tear production and corneal nerve fiber density are significantly reduced in the *Aire* KO mouse model (beginning at 5 weeks; Efraim et al., 2020) similar to human patients suffering from dry eye disease, e.g., due to Sjögren syndrome (Li et al., 2021; Navone et al., 2005), an outcome that strongly correlates with loss of active lacritin in human tears (McNamara et al., 2016).

To test for changes in innervation, corneas isolated from the four treatment groups at day 15 were immunostained for growth-associated protein 43 (GAP43), a marker of remodeling axons (Martin and Bazan, 1992), along with two common sensory neuropeptides, substance P (SP) and calcitonin gene-related protein (CGRP). SP and CGRP are differentially expressed to carry out discrete functions. SP is released in response to trigeminal activation to modulate tear secretion and goblet cell function (Kovács et al., 2005). Notably, physiological levels of SP promote corneal epithelial homeostasis and wound healing (Gaddipati et al., 2016; Suvas, 2017), while elevated levels promote inflammation (Chen et al., 2022). CGRP is a predominately anti-inflammatory neuropeptide involved in multiple homeostatic processes, including corneal epithelial regeneration and regulation of vasculature (Mikulec and Tanelian, 1996; Uusitalo et al., 1989). As shown in the whole-mount images in Figure 2A, WT corneas showed extensive innervation by GAP43+ nerve fibers expressing SP and/or CGRP (Figures 2A, 2B, and S2), consistent with the constant remodeling and functionality of corneal nerves (Martin and Bazan, 1992). In contrast to WT, nerve density was dramatically reduced in the untreated and PBS-treated *Aire* KO corneas, indicating that lubrication alone is not sufficient to maintain a functional nerve supply (Figure 2A). Strikingly, however, Lacripep-treated corneas showed extensive innervation throughout the tissue, with the density of highly branched GAP43+ nerve fibers expressing SP and CGRP being nearly equivalent to that of the WT controls (Figures 2A, 2B, and S2). Thus, Lacripep treatment successfully regenerates the sensory nerve supply to the inflamed cornea during disease progression.

Lacripep re-establishes functional corneal nerve-epithelial interactions during dry eye disease progression

Given that nerve-epithelial interactions are essential for mediating physiological tear secretion, we next assessed innervation to corneal epithelial cell layers at 2 weeks of treatment (day 15, age 7 weeks) through immunofluorescent analysis. As shown in Figure 2C, the corneal epithelium of untreated and PBS-treated mice were highly deficient in axons compared with the extensively innervated WT controls (Figures 2C and 2D). In contrast, innervation of Lacripep-treated epithelial cell layers resembled that of WT tissue, with TUBB3+ axons extending apically through the epithelium to reach the most superficial cells (Figures 2C and 2D). Thus, the reduced epithelial innervation at 5 weeks is effectively restored through sustained Lacripep treatment.

Next, we questioned the timing of epithelial reinnervation in response to Lacripep treatment by analyzing the nerve supply at the 7-day time point (age 6 weeks) through 3D imaging of intact whole-mount corneas (Figure 3A). As shown in Figure 3B, PBS-treated *Aire* KO corneal epithelia showed a severe reduction in innervation at day 7, with the central cornea possessing only 18% of the nerve density of WT tissue (Figure 3C), an outcome that remained at this level over the 2-week treatment window (see Figure 2). In contrast, corneas treated with Lacripep exhibited significantly greater innervation at 7 days, reaching 45% of the nerve density of WT tissue (Figures 3B and 3C), with levels returning to that of WT cornea by day 15 (see Figure 2). Consistent with Lacripep promoting nerve regeneration rather than nerve maintenance, Lacripep-treated *Aire* KO corneas displayed a greater proportion of newly regenerating GAP43+ (TUBB3−) nerves relative to GAP43+ TUBB3+ nerves than the WT corneas (Figures 3B and 3C). Specifically, the central corneas of Lacripep-treated KO mice were populated with 50% GAP43+ nerves and 26% GAP43+ TUBB3+ nerves while the

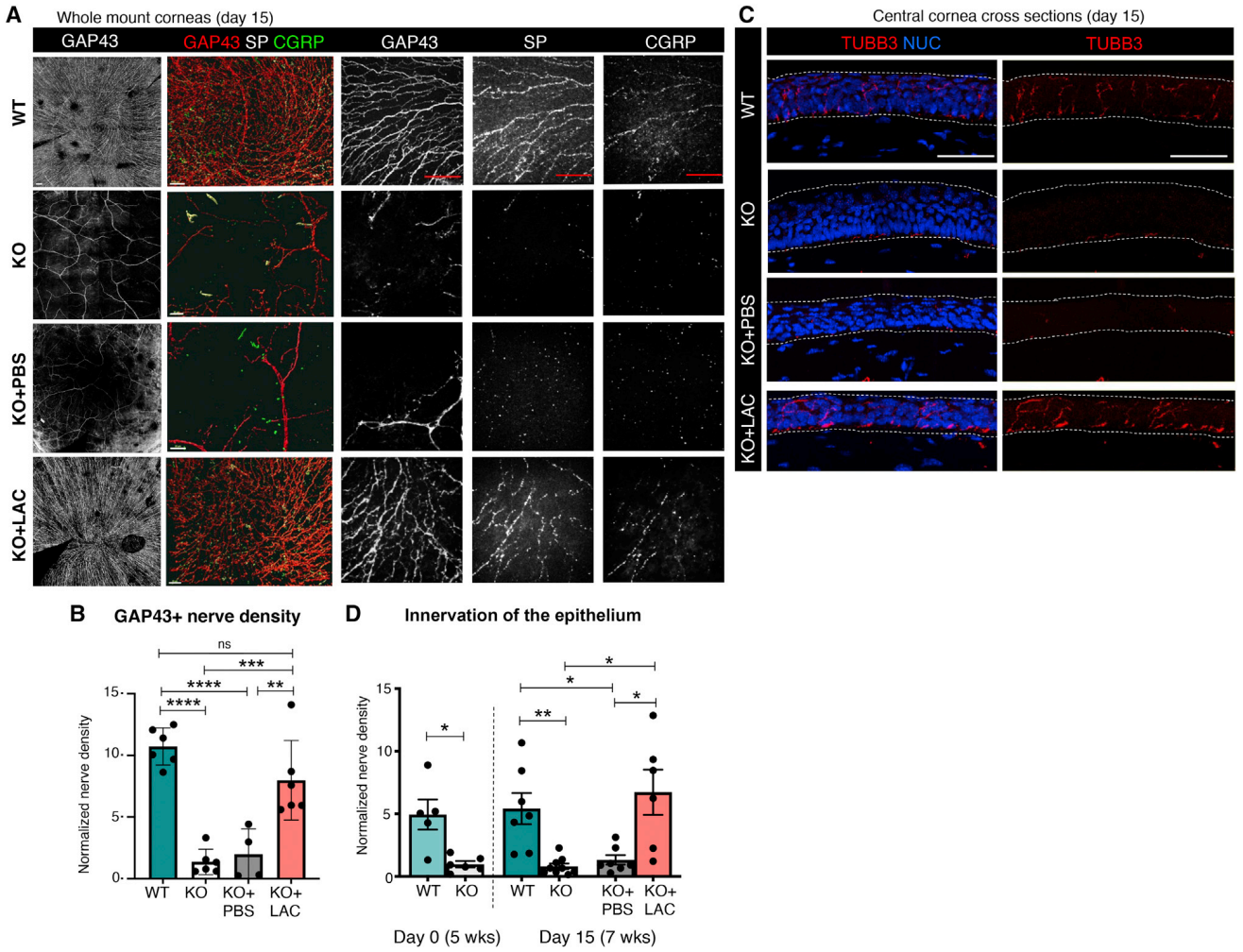

Figure 2. Sensory innervation of the desiccated cornea is restored in response to Lacripep treatment

(A) 3D projections of nerve fibers across the peripheral and central regions of WT, untreated, and PBS- or Lacripep-treated *Aire* KO cornea (whole-mount). Nerves were immunolabeled for the remodeling neuronal marker GAP43, and sensory neurotransmitters substance P (SP) and calcitonin gene-related peptide (CGRP). Scale bars, 70 μm for whole-mount sections (far left, gray), 30 μm for the GAP43, SP, CGRP combined image, 50 μm for GAP43, SP, or CGRP only images.

(B) Quantification of GAP43+ nerves in WT, and untreated/treated *Aire* KO corneas.

(C) Central corneal cross-sections (20 μm) were immunolabeled for the pan-neuronal marker TUBB3 and nuclei (NUC). Scale bars, 50 μm.

(D) Quantification of TUBB3+ nerves in the central corneal epithelium of WT, untreated and treated *Aire* KO. Scale bars, 50 μm. *$p < 0.05$, **$p < 0.01$, ***$p < 0.001$, ****$p < 0.0001$; n.s., not significant. Data in (B) were subjected to a one-way analysis of variance with a post-hoc Tukey's test. In (D), a Student's t test was applied to WT versus KO at day 0 and a one-way analysis of variance with a post-hoc Tukey's test was applied to day 15. Each dot in the bar graph represents a biological replicate. All data are expressed as mean + SD. $n > 4$ mice per group. See also Figure S2.

WT tissue showed 43% and 37%, respectively (Figure 3C). Of note, the pro-regenerative cellular changes after axon injury result in neurons switching from an active, electrically transmitting state back to an electrically silent, growth-competent state (Mahar and Cavalli, 2018; Quadrato and Di Giovanni, 2013) thereby likely impairing increased tear production at the 7-day time point for Lacripep-treated mice compared with untreated *Aire* KO controls (Figure 1B).

We next determined the extent of functional reinnervation of the cornea at day 7 by assessing the distribution of sensory nerve endings (nerve terminals) within the epithelial layers in Lacripep-treated *Aire* KO corneas compared with WT and PBS-treated *Aire* KO controls (Figure 3D). Sensory nerve terminals within the corneal epithelium respond to changes in the thickness and stability of the tear film to promote tear secretion, while also triggering epithelial responses to restore homeostasis through the release of neurotransmitters. Using 3D imaging and topographical reconstruction by IMARIS, we identified an extensive array of intraepithelial sensory nerve terminals within the WT controls (78 per 0.1 mm^2) contrasting with the severely reduced numbers found in PBS-treated *Aire* KO (Figures 3D and 3E). However, Lacripep-treated *Aire* KO epithelia showed a significant increase in nerve terminals (50 per 0.1 mm^2), indicating that nerve-epithelial crosstalk was being re-established.

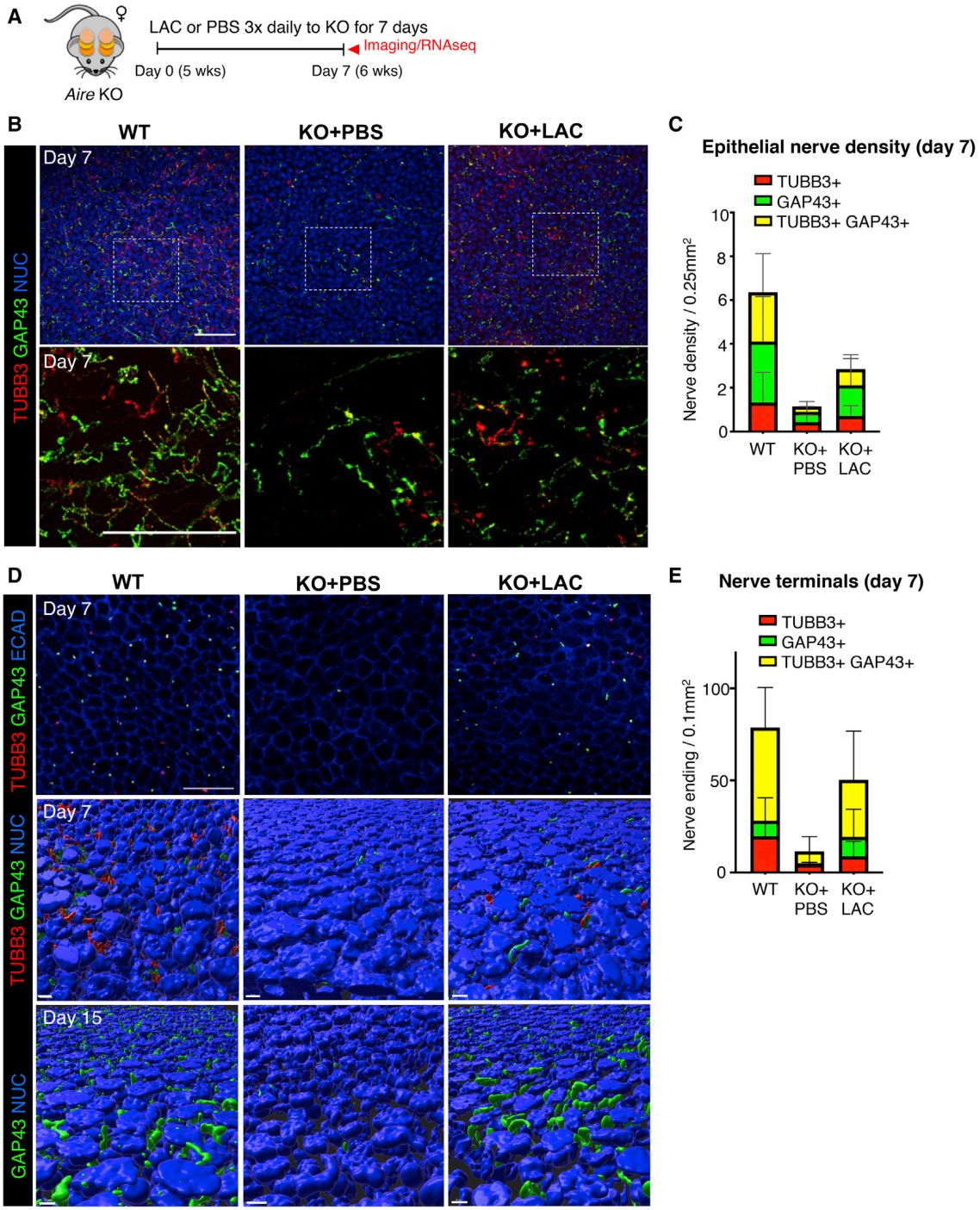

Figure 3. Lacripep re-establishes functional corneal nerve-epithelial interactions during dry eye disease progression

(A) Schematic of the treatment regimen showing data collection time points for RNA-seq and tissue analyses.

(B–C) Immunofluorescent analysis (B) and quantification (C) of regenerating nerves in the corneal epithelium at day 7. The graph in (C) shows the relative proportion of newly regenerating GAP43+ nerves in the central cornea. Scale bars, 50 μm.

(D) 3D reconstruction of whole-mount immunofluorescent images of newly regenerating (GAP43+) and existing (TUBB3+) intraepithelial nerve terminals at days 7 (upper panel) and 15 (lower panel) in the corneal epithelium.Scale bars, 25 μm (IF),10 μm (3D reconstruction).

(E) Graph showing relative proportion of GAP43+, GAP43 + TUBB3+, and TUBB3+ nerve terminals in the central cornea at day 7. NUC, nuclei. All data are expressed as mean + SD. n > 4 mice per group.

Consistent with the activation of nerve regeneration rather than nerve maintenance, the proportion of the sensory nerve terminals that expressed GAP43, as opposed to TUBB3 alone, in the Lacripep-treated corneas, was significantly greater than WT ($p < 0.05$) and PBS-treated tissue ($p < 0.05$; Figures 3D and 3E). Moreover, at day 15 the total number of nerve terminals in the Lacripep-treated *Aire* KO cornea epithelium was similar to that of WT controls, highlighting the extensive recovery of innervation taking place during disease progression (Figure 3D). Collectively, our data illustrate the therapeutic efficiency of Lacripep as a topical dry eye treatment capable of regenerating functional corneal nerves and nerve-epithelial connections required for ocular integrity, signaling, and tear secretion.

Lacripep activates master regulators of nerve regeneration

Finally, we questioned the potential mechanism by which Lacripep restores the nerve supply. Lacritin and Lacripep bind and activate syndecan-1 (SDC1), a transmembrane heparan sulfate proteoglycan enriched in the corneal epithelium, which has been shown to increase epithelial cell proliferation and migration *in vitro* (Lee et al., 2020; Ma et al., 2006). SDC1 is also heavily involved in corneal nerve regeneration after injury (Pal-Ghosh et al., 2017), with *Sdc1*-deficient mice exhibiting a profound reduction in corneal innervation after ocular damage, which is subsequently followed by corneal pathologies consistent with dry eye (Pal-Ghosh et al., 2017). Thus, we first confirmed that SDC1 remains expressed in the epithelium during dry eye disease progression through application of *in situ* hybridization (RNAscope) to healthy and diseased corneas at age 7 weeks. As shown in Figure 4A, *Sdc1* transcripts were highly enriched in the basal and suprabasal cell populations of the WT corneas in a manner consistent with previous studies (Stepp et al., 2002). Similarly, we found that *Sdc1* transcripts were also abundantly located in the basal and suprabasal cells of the *Aire* KO corneal epithelium (Figure 4A), thus demonstrating that SDC1-Lacripep interactions within the epithelium can take place during dry eye disease progression.

To identify potential downstream targets of Lacripep treatment, we elucidated changes in corneal gene expression and signaling pathways at the day 7 time point through RNA-seq of the intact cornea (including epithelium, stroma, nerve fibers, and immune cells). Principal-component analysis identified major transcriptional differences between each treatment group (Figure S3A). Strikingly, differential gene expression analysis (Love et al., 2014) ($p_{adj} < 0.05$; 2-fold change cutoff) of Lacripep- versus PBS-treated corneas revealed an extensive alteration in gene expression that was predominantly associated with increased transcription, with 818 genes being significantly upregulated while only 15 were downregulated (Figure 4B; Table S3). Subsequent analysis yielded enriched gene sets that were highly associated with neuronal gene ontology terms, e.g., synapse ($p = 3.6E{-}47$), visual perception ($p = 5.8E{-}49$), neuron projection ($p = 2.1E{-}29$), and response to stimulus ($p = 1.8E{-}19$) (Figure 4C; Table S4). These included cohorts of genes expressed by nerves and/or corneal epithelial cells involved in axonogenesis and axon guidance, e.g., *Neurod2*, *Cntn4*, ephrins (*Epha5*, *Epha7*, *Epha8*), and semaphorins (*Sema6a*, *Sema7a*); synapse formation and function, e.g., synaptic vesicle membrane proteins (*Syt1*; synaptophysin-*Syp*) and synaptic vesicle exocytosis regulators (*Rims1*, *Rims2*); neuronal signaling, e.g., GABA receptors (*Gabra2*, *Gabrr1*), glutamate receptors (*Gria2*, *Gria4)*, and G protein signal-transducing mediators (*Gnb3*, *Gng4*); and neurotransmitter transport, e.g., glutamate transporters (*Slc17a7*) and GABA transporters (*Slc6a1*, *Slc32a1*) (Figure 4D; Table S5). Analysis of corneas treated with Lacripep or PBS versus untreated corneas further emphasized the ability of Lacripep and not PBS alone to induce transcription of neuronal gene sets (Figure S3B). Combined, these data clearly demonstrate that Lacripep positively promotes neuroregeneration by upregulating a gene signature associated with axon migration, synapse formation, and neuronal-epithelial signaling.

To identify candidate transcription factors (TFs) that regulate these gene sets, we performed TF-gene target regulatory network analysis using iRegulon (Janky et al., 2014). iRegulon identifies TF-binding motifs that are enriched in the genomic regions of a query gene set and predicts TFs that bind to them. This revealed an abundant upregulation of target gene sets from three top master transcriptional regulators, RE1 silencing transcription factor (*Rest*, 184 genes), ISL LIM homeobox 1 (*Isl1*, 394 genes), and Ras-responsive element-binding protein 1 (*Rreb1*, 254 genes) (Figure S3C and 4E; Table S5). ISL1 plays an essential role in the generation of sensory and sympathetic neurons (Sun et al., 2008; Zhang et al., 2018), REST is a master regulator of neurogenesis that plays a role in modulating synaptic plasticity (Ballas and Mandel, 2005; Hwang and Zukin, 2018; Rodenas-Ruano et al., 2012) and RREB1 regulates axon injury (Farley et al., 2018). Notably, we identified a significant number of genes per gene set that are uniquely regulated by one of the three different TFs (Figure 4E; Table S6). This was particularly the case for *Isl1*, a TF previously shown to be enriched in the limbal cells (Nieto-Miguel et al., 2011) and corneal sensory nerves (Bouheraoua et al., 2019), where 47% of gene targets (185 out of 394) did not overlap with the other TFs, compared with 29% and 28% for *Rest* and *Rreb1*, respectively (Figure 4E; Table S5). The *Isl1* exclusive gene set was also extensively enriched in genes involved with functional and structural nerve-mediated processes, including visual perception ($p = 3.5E{-}27$, e.g., *Capb4*, *Vsx1*), response to stimulus ($p = 9.7E{-}19$; e.g., *Slc17a7*, *Ush2a*), synapse ($p = 9.4E{-}8$, e.g., *Magi2*, *Synpr*), and neuron projection ($p = 6.4E{-}6$, e.g., *Cdh23*, *Kif1a*) (Figure 4F; Table S6). Although the identified gene sets found to be exclusively regulated by *Rest* and *Rreb1* were less extensive than that of Isl1, each of the three TFs regulated specific genes involved in synapse formation and function (Figure 4F), suggesting that *Isl1*, *Rest*, and *Rreb1* jointly regulate nerve-epithelial communication in response to Lacripep.

Thus, together these data suggest that Lacripep regenerates sensory nerves and re-establishes nerve-epithelial communication during dry eye disease progression through upregulation of master regulators of neuronal-associated gene sets.

DISCUSSION

To date, none of the dry eye therapies, including those currently in clinical trials, have been shown to promote the comprehensive restoration of corneal structure and function at the cellular and

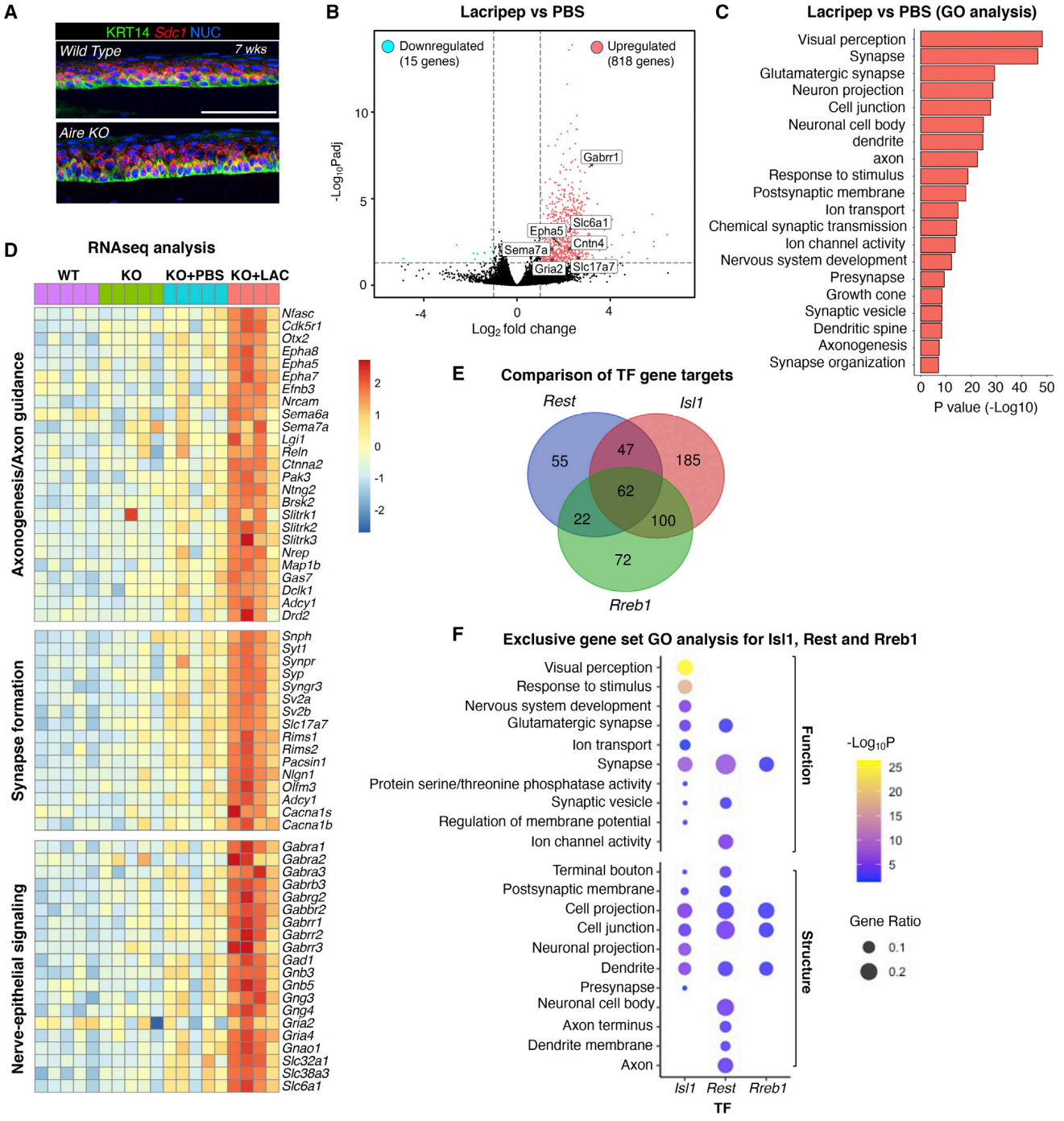

Figure 4. Lacripep activates master regulators of nerve regeneration in the desiccated cornea

(A) RNA transcripts for syndecan-1 (*Sdc1*), co-receptor for Lacripep, in the basal and suprabasal epithelial cells of WT and *Aire* KO cornea at age 7 weeks. Scale bar, 50 μm.

(B) Volcano plot of differentially expressed corneal genes in response to Lacripep versus PBS treatment at day 7. Red and blue dots represent genes significantly upregulated and downregulated, respectively (log2 FC ≥1 and padj <0.05).

(C) Gene ontology (GO) analysis highlighting upregulated pathways in Lacripep- versus PBS-treated *Aire* KO corneas.

(D) Heatmap featuring Lacripep-induced upregulated genes associated with axonogenesis, axon guidance, nerve-epithelial signaling, and synapse formation at day 7 of treatment.

(E) Venn diagram of the top transcription factors *Isl1*, *Rest*, and *Rreb1* regulon targets upregulated in response to Lacripep. Normalized enrichment score > 3; #Targets > 100.

(F) GO analysis of the exclusive target gene sets for each TF in (E), highlighting individual and combined roles in the regulation of function- and structure-based neuronal processes. $p < 0.05$. See also Figure S3 and Tables S1, S2, S3, S4, S5, and S6.

tissue level in pre-clinical animal models. Indeed, current medications for multiple ocular surface diseases serve to inhibit inflammation but fail to act on the tissue itself to retain or regain structure and function. Here, we demonstrate that Lacripep treatment reverses the multifaceted pathogenesis of dry eye disease through its prosecretory, pro-regenerative, and neurotrophic functions. Using a murine model that recapitulates many of the features of dry eye disease, we show that Lacripep restores the structural and functional integrity of the cornea and basal progenitor cell identity by promoting functional reinnervation of the epithelium, thereby serving to disrupt disease development and support active wound healing. Furthermore, we show that this outcome occurs in the presence of chronic inflammation, thus indicating that the regeneration and reinnervation of inflamed tissues can occur in the diseased context.

Loss of corneal nerves is an established clinical consequence of dry eye pathogenesis in Sjögren syndrome, diabetes (Mocan et al., 2006), rheumatoid arthritis (Villani et al., 2008), scleroderma (Szalai et al., 2021), thyroid-associated disorders (e.g., thyroid-associated ophthalmopathy) (Wu et al., 2019), and chronic graft-versus-host disease (Steger et al., 2015). However, despite this, the clinically approved therapeutics utilized to treat dry eye to date are directed at dampening inflammation, but none have been shown to promote the restoration of corneal nerves or to regenerate tissue. With recent studies showing a vital role for T cell signaling pathways in promoting the stability of ocular surface homeostasis and the wound repair process (Altshuler et al., 2021; Liu and Li, 2021), reducing immune cell infiltration and/or altering their function may inhibit cornea/nerve regeneration. In contrast, the highly utilized anti-inflammatory drug cyclosporin A has been shown to retard the regeneration of surgically transected nerves (Namavari et al., 2012). These outcomes have consequently fueled a growing interest in the development of novel therapies that target disrupted innervation. To date, several factors with neuroregenerative potential have been tested in animal models, including corneal matrix repair product cacicol (Alcalde et al., 2015), insulin growth factor-1 (Wang et al., 2014), the neuropeptide pituitary adenylate cyclase-activating polypeptide (Fukiage et al., 2007), pigment epithelium-derived factor (Cortina et al., 2012), and N-(1-acetylpiperidin-4-yl)-4-fluorobenzamide (FK962) (Yabuta et al., 2012), but results have been limited. More recently in preclinical and clinical studies for treating neurotrophic keratitis, an uncommon degenerative disease of the cornea resulting in denervation, breakdown of the epithelium, ulceration, and perforation, (Bonini et al., 2018; Pflugfelder et al., 2020), recombinant nerve growth factor (cenegermin) stimulated the reinnervation of rabbit corneas after refractive surgery (Gong et al., 2021) and boosted corneal wound healing in human patients. However, in controlled clinical studies it has failed to show significant benefit over vehicle (artificial tears) in terms of corneal sensitivity or visual acuity (Deeks and Lamb, 2020). Moreover, its direct contribution to the regeneration and reinnervation of corneas from patients with neurotrophic keratitis and whether it can resolve dry eye pathologies in the setting of chronic inflammation are yet to be addressed.

Our study highlights a significant link between neuroregeneration and the restoration of progenitor cell identity in a model of chronic, autoimmune-mediated dry eye. Multiple studies in other organ systems, such as the salivary glands (Emmerson et al., 2018), tooth (Zhao et al., 2014), and skin (Huang et al., 2021; Xiao et al., 2015), have established a critical role for nerves in the regulation of tissue structure and function, as well as progenitor cell maintenance. In the cornea, mouse models of both chemically and physically induced denervation (Lambiase et al., 2012; Ueno et al., 2012) have implicated sensory innervation as a regulator of progenitor cell identity, as determined by a reduction in the expression of epithelial progenitor cell markers, such as p63 (Ueno et al., 2012), an outcome that can be partially reversed by topical nerve growth factor treatment (Lambiase et al., 2012). Yet, the impact of denervation and reinnervation on the differentiation status of basal progenitors has not been addressed. Our data suggest that Lacripep's restorative effects on corneal innervation are mediated through its impact on epithelial cell identity/differentiation. Further studies are needed to identify the specific signaling systems activated by Lacripep and the mechanism whereby sensory innervation regulates epithelial progenitor identity and cell fate.

Although the precise mechanism by which Lacripep stimulates corneal reinnervation remains unclear, its known interaction with SDC1 suggests that Lacripep mediates its neuroregenerative effects via binding and activating SDC1. Indeed, the nerve phenotype of the *Aire* KO cornea during dry eye disease progression strongly resembles that of the injured *Sdc1*-KO cornea (Pal-Ghosh et al., 2017), as shown by the substantial reduction in intraepithelial nerve terminals and reinnervation. However, little is known about the downstream pathways that mediate neuroregeneration in response to SDC1. Our RNA-seq analysis of the *Aire* KO cornea containing all cell types provides insight into the potential mechanism of corneal reinnervation through the identification of three master regulators of the highly enriched neuronal gene sets, namely *Isl1*, *Rest*, and *Rreb1*, potentially directing Lacripep-induced nerve remodeling, neurite outgrowth, and synapse formation and function. Specifically, these factors have been reported to orchestrate processes, such as neurogenesis, synaptogenesis, and/or axon regeneration (Ballas and Mandel, 2005; Farley et al., 2018; Hwang and Zukin, 2018; Rodenas-Ruano et al., 2012; Sun et al., 2008; Zhang et al., 2018). In addition, REST acts as a critical factor linking neuronal activity to the activation of intrinsic homeostasis and restoring physiological levels of activity throughout the entire neuronal network (Pozzi et al., 2013). Furthermore, in addition to regulating innervation, ISL1, RREB1, and REST are also involved in stem cell/progenitor maintenance, epithelial differentiation, and proliferation, as well as epithelial architecture and integrity (Baechler et al., 2015; Kim et al., 2019; Morgani et al., 2021; Singh et al., 2008; Su et al., 2019), suggesting Lacripep delivers regenerative instructions to the epithelium to coordinate the regulation of tissue structure and cell identity. Thus, Lacripep may act by fine-tuning the nerves and the epithelium via these TFs to achieve functional reinnervation.

In summary, our study highlights Lacripep as a therapeutic capable of resolving ocular damage through promoting functional reinnervation of the cornea. Future studies exploring Lacripep's effects at the cellular level will allow us to identify and target specific signaling pathways essential for corneal re-innervation and restoration in patients with dry eye and other vision-threatening ocular surface disorders that impact corneal

nerves (e.g., herpes simplex virus, interstitial keratitis, and neurotrophic keratitis).

Limitations of the study

Limitations of our study include variation in the disease severity of the *Aire* KO mouse model, which could affect the treatment response. In addition, we were unable to track innervation of individual mouse corneas over time, which prevented us from directly assessing nerve regeneration in response to Lacripep treatment compared with baseline. Finally, the duration and extent of the effect of Lacripep on the cornea after Lacripep treatment is discontinued remains unknown. As *Aire* KO mice provide a model of chronic ocular inflammatory disease, we reasoned that ongoing treatment is necessary to maintain innervation and corneal function. Future experiments are necessary to address this question, as well as to elucidate the mechanism(s) of action by which Lacripep restores corneal nerves.

STAR★METHODS

Detailed methods are provided in the online version of this paper and include the following:

- KEY RESOURCES TABLE
- RESOURCE AVAILABILITY
  - Lead contact
  - Materials availability
  - Data and code availability
- EXPERIMENTAL MODEL AND SUBJECT DETAILS
  - Animals
- METHOD DETAILS
  - Treatment regimen
  - Analysis of epithelial barrier function
  - Tear secretion measurements
  - Tissue processing and immunohistological analyses
  - *In situ* hybridization
  - Image analysis
  - RNA isolation and RNAseq library generation
  - RNAseq analysis
- QUANTIFICATION AND STATISTICAL ANALYSIS

SUPPLEMENTAL INFORMATION

Supplemental information can be found online at https://doi.org/10.1016/j.celrep.2022.111307.

ACKNOWLEDGMENTS

The authors would like to thank Dr. Gordon Laurie (University of Virginia) for providing the synthetic tear protein Lacripep. The authors would also like to thank Drs. John Whitelock, Alison May, Ophir Klein, Jeffrey Bush, and Matilda Chan for their constructive input toward this manuscript as well as the sharing of reagents and instruments. This work was supported by the following funding sources: National Eye Institute grants R01EY025980 (to S.M.K. and N.A.M.), R01EY027392 (to S.M.K.), and R01EY033040 (to S.M.K. and N.A.M.).

AUTHOR CONTRIBUTIONS

Conceptualization, Y.E., F.Y.T.C., N.A.M., and S.M.K.; methodology, Y.E., F.Y.T.C., K.N.C., E.A.G., N.A.M., and S.M.K.; investigation, Y.E., F.Y.T.C., K.N.C., and E.A.G.; visualization, Y.E., F.Y.T.C., K.N.C., and S.M.K.; funding acquisition, S.M.K. and N.A.M.; project administration, S.M.K. and N.A.M.; supervision, S.M.K. and N.A.M.; writing – original draft, Y.E., F.Y.T.C., N.A.M., and S.M.K.; writing – review & editing, Y.E., F.Y.T.C., N.A.M., and S.M.K.

DECLARATION OF INTERESTS

N.A.M. currently serves on the Medical Advisory Board for TearSolutions. All other authors declare no competing interests.

Received: May 11, 2022
Revised: July 17, 2022
Accepted: August 11, 2022
Published: August 30, 2022

REFERENCES

Alcalde, I., Íñigo-Portugués, A., Carreño, N., Riestra, A.C., and Merayo-Lloves, J.M. (2015). Effects of new biomimetic regenerating agents on corneal wound healing in an experimental model of post-surgical corneal ulcers. Arch. Soc. Esp. Oftalmol. *90*, 467–474.

Altshuler, A., Amitai-Lange, A., Tarazi, N., Dey, S., Strinkovsky, L., Hadad-Porat, S., Bhattacharya, S., Nasser, W., Imeri, J., Ben-David, G., et al. (2021). Discrete limbal epithelial stem cell populations mediate corneal homeostasis and wound healing. Cell Stem Cell *28*, 1248–1261.e8.

Baechler, B.L., McKnight, C., Pruchnicki, P.C., Biro, N.A., and Reed, B.H. (2015). Hindsight/RREB-1 functions in both the specification and differentiation of stem cells in the adult midgut of Drosophila. Biol. Open *5*, 1–10. https://doi.org/10.1242/bio.015636.

Ballas, N., and Mandel, G. (2005). The many faces of REST oversee epigenetic programming of neuronal genes. Curr. Opin. Neurobiol. *15*, 500–506.

Blighe, K., Rana, S., and Lewis, M. (2019). EnhancedVolcano: publication-ready volcano plots with enhanced colouring and labelin. R-Package, pp. 1–8.

Bonini, S., Lambiase, A., Rama, P., Sinigaglia, F., Allegretti, M., Chao, W., Mantelli, F., REPARO Study Group; Aragona, P., and Geerling, G. (2018). Phase II randomized, double-masked, vehicle-controlled trial of recombinant human nerve growth factor for neurotrophic keratitis. Ophthalmology *125*, 1332–1343.

Boonekamp, K.E., Kretzschmar, K., Wiener, D.J., Asra, P., Derakhshan, S., Puschhof, J., López-Iglesias, C., Peters, P.J., Basak, O., and Clevers, H. (2019). Long-term expansion and differentiation of adult murine epidermal stem cells in 3D organoid cultures. Proc. Natl. Acad. Sci. USA *116*, 14630–14638. https://doi.org/10.1073/pnas.1715272116.

Bouheraoua, N., Fouquet, S., Marcos-Almaraz, M.T., Karagogeos, D., Laroche, L., and Chédotal, A. (2019). Genetic analysis of the organization, development, and plasticity of corneal innervation in mice. J. Neurosci. *39*, 1150–1168. https://doi.org/10.1523/JNEUROSCI.1401-18.2018.

Chen, F.Y., Lee, A., Ge, S., Nathan, S., Knox, S.M., and McNamara, N.A. (2017). Aire-deficient mice provide a model of corneal and lacrimal gland neuropathy in Sjögren's syndrome. PLoS One *12*, e0184916. https://doi.org/10.1371/journal.pone.0184916.

Chen, F.Y., Gaylord, E., McNamara, N., and Knox, S. (2018a). Deciphering molecular and phenotypic changes associated with early autoimmune disease in the aire-deficient mouse model of Sjögren's syndrome. Int. J. Mol. Sci. *19*, E3628. https://doi.org/10.3390/ijms19113628.

Chen, S., Zhou, Y., Chen, Y., and Gu, J. (2018b). fastp: an ultra-fast all-in-one FASTQ preprocessor. Bioinformatics *34*, i884–i890. https://doi.org/10.1093/bioinformatics/bty560.

Chen, Y., Wang, S., Alemi, H., Dohlman, T., and Dana, R. (2022). Immune regulation of the ocular surface. Exp. Eye Res. *218*, 109007. https://doi.org/10.1016/j.exer.2022.109007.

Cortina, M.S., He, J., Li, N., Bazan, N.G., and Bazan, H.E.P. (2012). Recovery of corneal sensitivity, calcitonin gene-related peptide–positive nerves, and increased wound healing induced by pigment epithelial–derived factor plus

docosahexaenoic acid after experimental surgery. Arch. Ophthalmol. *130*, 76–83.

Deeks, E.D., and Lamb, Y.N. (2020). Cenegermin: a review in neurotrophic keratitis. Drugs *80*, 489–494.

Di Girolamo, N., Bobba, S., Raviraj, V., Delic, N.C., Slapetova, I., Nicovich, P.R., Halliday, G.M., Wakefield, D., Whan, R., and Lyons, J.G. (2015). Tracing the fate of limbal epithelial progenitor cells in the murine cornea. Stem Cell. *33*, 157–169. https://doi.org/10.1002/stem.1769.

Dobin, A., Davis, C.A., Schlesinger, F., Drenkow, J., Zaleski, C., Jha, S., Batut, P., Chaisson, M., and Gingeras, T.R. (2013). STAR: ultrafast universal RNA-seq aligner. Bioinformatics. https://doi.org/10.1093/bioinformatics/bts635.

Efraim, Y., Chen, F.Y.T., Stashko, C., Cheong, K.N., Gaylord, E., McNamara, N., and Knox, S.M. (2020). Alterations in corneal biomechanics underlie early stages of autoimmune-mediated dry eye disease. J. Autoimmun. *114*, 102500. https://doi.org/10.1016/j.jaut.2020.102500.

Emmerson, E., May, A.J., Berthoin, L., Cruz-Pacheco, N., Nathan, S., Mattingly, A.J., Chang, J.L., Ryan, W.R., Tward, A.D., and Knox, S.M. (2018). Salivary glands regenerate after radiation injury through SOX2-mediated secretory cell replacement. EMBO Mol. Med. *10*, e8051. https://doi.org/10.15252/emmm.201708051.

Farley, J.E., Burdett, T.C., Barria, R., Neukomm, L.J., Kenna, K.P., Landers, J.E., and Freeman, M.R. (2018). Transcription factor Pebbled/RREB1 regulates injury-induced axon degeneration. Proc. Natl. Acad. Sci. USA *115*, 1358–1363.

Fukiage, C., Nakajima, T., Takayama, Y., Minagawa, Y., Shearer, T.R., and Azuma, M. (2007). PACAP induces neurite outgrowth in cultured trigeminal ganglion cells and recovery of corneal sensitivity after flap surgery in rabbits. Am. J. Ophthalmol. *143*, 255–262.

Gaddipati, S., Rao, P., Jerome, A.D., Burugula, B.B., Gerard, N.P., and Suvas, S. (2016). Loss of neurokinin-1 receptor alters ocular surface homeostasis and promotes an early development of herpes stromal keratitis. J. Immunol. *197*, 4021–4033. https://doi.org/10.4049/jimmunol.1600836.

Georgiev, G.A., Gh, M.S., Romano, J., Dias Teixeira, K.L., Struble, C., Ryan, D.S., Sia, R.K., Kitt, J.P., Harris, J.M., Hsu, K.-L., et al. (2021). Lacritin proteoforms prevent tear film collapse and maintain epithelial homeostasis. J. Biol. Chem. *296*, 100070. https://doi.org/10.1074/jbc.RA120.015833.

Gong, Q., Zhang, S., Jiang, L., Lin, M., Xu, Z., Yu, Y., Wang, Q., Lu, F., and Hu, L. (2021). The effect of nerve growth factor on corneal nerve regeneration and dry eye after LASIK. Exp. Eye Res. *203*, 108428.

Huang, D.W., Sherman, B.T., and Lempicki, R.A. (2009). Systematic and integrative analysis of large gene lists using DAVID bioinformatics resources. Nat. Protoc. *4*, 44–57. https://doi.org/10.1038/nprot.2008.211.

Huang, S., Kuri, P., Aubert, Y., Brewster, M., Li, N., Farrelly, O., Rice, G., Bae, H., Prouty, S., Dentchev, T., et al. (2021). Lgr6 marks epidermal stem cells with a nerve-dependent role in wound re-epithelialization. Cell Stem Cell *28*, 1582–1596.e6. https://doi.org/10.1016/j.stem.2021.05.007.

Hwang, J.-Y., and Zukin, R.S. (2018). REST, a master transcriptional regulator in neurodegenerative disease. Curr. Opin. Neurobiol. *48*, 193–200.

Janky, R., Verfaillie, A., Imrichová, H., Van de Sande, B., Standaert, L., Christiaens, V., Hulselmans, G., Herten, K., Naval Sanchez, M., Potier, D., et al. (2014). iRegulon: from a gene list to a gene regulatory network using large motif and track collections. PLoS Comput. Biol. *10*, e1003731.

Kim, E., Jiang, M., Huang, H., Zhang, Y., Tjota, N., Gao, X., Robert, J., Gilmore, N., Gan, L., and Que, J. (2019). Isl1 regulation of Nkx2. 1 in the early foregut epithelium is required for trachea-esophageal separation and lung lobation. Dev. Cell *51*, 675–683.e4.

Kolde, R. (2015). Pheatmap : pretty heatmaps. R Packag. Version 1.0.8 1, pp. 1–7.

Kovács, I., Ludány, A., Kőszegi, T., Fehér, J., Kovács, B., Szolcsányi, J., and Pintér, E. (2005). Substance P released from sensory nerve endings influences tear secretion and goblet cell function in the rat. Neuropeptides *39*, 395–402.

Labbé, A., Liang, Q., Wang, Z., Zhang, Y., Xu, L., Baudouin, C., and Sun, X. (2013). Corneal nerve structure and function in patients with non-sjögren dry eye: clinical correlations. Invest. Ophthalmol. Vis. Sci. *54*, 5144–5150. https://doi.org/10.1167/iovs.13-12370.

Lambiase, A., Aloe, L., Mantelli, F., Sacchetti, M., Perrella, E., Bianchi, P., Rocco, M.L., and Bonini, S. (2012). Capsaicin-induced corneal sensory denervation and healing impairment are reversed by NGF treatment. Invest. Ophthalmol. Vis. Sci. *53*, 8280–8287. https://doi.org/10.1167/iovs.12-10593.

Lee, C., Edman, M.C., Laurie, G.W., Hamm-Alvarez, S.F., and MacKay, J.A. (2020). Biosynthesized multivalent lacritin peptides stimulate exosome production in human corneal epithelium. Int. J. Mol. Sci. *21*, E6157. https://doi.org/10.3390/ijms21176157.

Lemp, M.A., Baudouin, C., Baum, J., Dogru, M., Foulks, G.N., Kinoshita, S., Laibson, P., McCulley, J., Murube, J., Pflugfelder, S.C., et al. (2007). The definition and classification of dry eye disease: report of the definition and classification subcommittee of the international Dry Eye WorkShop. Ocul. Surf.

Li, F., Zhang, Q., Ying, X., He, J., Jin, Y., Xu, H., Cheng, Y., and Zhao, M. (2021). Corneal nerve structure in patients with primary Sjögren's syndrome in China. BMC Ophthalmol. *21*, 211. https://doi.org/10.1186/s12886-021-01967-7.

Liu, J., and Li, Z. (2021). Resident innate immune cells in the cornea. Front. Immunol. *12*, 620284.

Love, M.I., Huber, W., and Anders, S. (2014). Moderated estimation of fold change and dispersion for RNA-seq data with DESeq2. Genome Biol. *15*, 550. https://doi.org/10.1186/s13059-014-0550-8.

Ma, P., Beck, S.L., Raab, R.W., McKown, R.L., Coffman, G.L., Utani, A., Chirico, W.J., Rapraeger, A.C., and Laurie, G.W. (2006). Heparanase deglycanation of syndecan-1 is required for binding of the epithelial-restricted prosecretory mitogen lacritin. J. Cell Biol. *174*, 1097–1106. https://doi.org/10.1083/jcb.200511134.

Mahar, M., and Cavalli, V. (2018). Intrinsic mechanisms of neuronal axon regeneration. Nat. Rev. Neurosci. *19*, 323–337. https://doi.org/10.1038/s41583-018-0001-8.

Martin, R.E., and Bazan, N.G. (1992). Growth-associated protein GAP-43 and nerve cell adhesion molecule in sensory nerves of cornea. Exp. Eye Res. *55*, 307–314. https://doi.org/10.1016/0014-4835(92)90195-X.

McNamara, N.A., Ge, S., Lee, S.M., Enghauser, A.M., Kuehl, L., Chen, F.Y.-T., Gallup, M., and McKown, R.L. (2016). Reduced levels of tear lacritin are associated with corneal neuropathy in patients with the ocular component of Sjögren's syndrome. Invest. Ophthalmol. Vis. Sci. *57*, 5237–5243. https://doi.org/10.1167/iovs.16-19309.

Mikulec, A.A., and Tanelian, D.L. (1996). CGRP increases the rate of corneal re-epithelialization in an in vitro whole mount preparation. J. Ocul. Pharmacol. Ther. *12*, 417–423. https://doi.org/10.1089/jop.1996.12.417.

Mocan, M.C., Durukan, I., Irkec, M., and Orhan, M. (2006). Morphologic alterations of both the stromal and subbasal nerves in the corneas of patients with diabetes. Cornea *25*, 769–773.

Morgani, S.M., Su, J., Nichols, J., Massagué, J., and Hadjantonakis, A.-K. (2021). The transcription factor Rreb1 regulates epithelial architecture, invasiveness, and vasculogenesis in early mouse embryos. Elife *10*, e64811.

Namavari, A., Chaudhary, S., Chang, J.-H., Yco, L., Sonawane, S., Khanolkar, V., Yue, B.Y., Sarkar, J., and Jain, S. (2012). Cyclosporine immunomodulation retards regeneration of surgically transected corneal nerves. Invest. Ophthalmol. Vis. Sci. *53*, 732–740.

Navone, R., Lunardi, C., Gerli, R., Tinazzi, E., Peterlana, D., Bason, C., Corrocher, R., and Puccetti, A. (2005). Identification of tear lipocalin as a novel autoantigen target in Sjögren's syndrome. J. Autoimmun. *25*, 229–234. https://doi.org/10.1016/j.jaut.2005.09.021.

Nieto-Miguel, T., Calonge, M., de la Mata, A., López-Paniagua, M., Galindo, S., de la Paz, M.F., and Corrales, R.M. (2011). A comparison of stem cell-related gene expression in the progenitor-rich limbal epithelium and the differentiating central corneal epithelium. Mol. Vis. *17*, 2102–2117.

Pal-Ghosh, S., Tadvalkar, G., and Stepp, M.A. (2017). Alterations in corneal sensory nerves during homeostasis, aging, and after injury in mice lacking the heparan sulfate proteoglycan syndecan-1. Invest. Ophthalmol. Vis. Sci. *58*, 4959–4975. https://doi.org/10.1167/iovs.17-21531.

Park, M., Richardson, A., Pandzic, E., Lobo, E.P., Whan, R., Watson, S.L., Lyons, J.G., Wakefield, D., and Di Girolamo, N. (2019). Visualizing the contribution of keratin-14+ limbal epithelial precursors in corneal wound healing. Stem Cell Rep. *12*, 14–28.

Pflugfelder, S.C., de Paiva, C.S., Li, D.-Q., and Stern, M.E. (2008). Epithelial–immune cell interaction in dry eye. Cornea *27*, 9–11.

Pflugfelder, S.C., Massaro-Giordano, M., Perez, V.L., Hamrah, P., Deng, S.X., Espandar, L., Foster, C.S., Affeldt, J., Seedor, J.A., Afshari, N.A., et al. (2020). Topical recombinant human nerve growth factor (cenegermin) for neurotrophic keratopathy: a multicenter randomized vehicle-controlled pivotal trial. Ophthalmology *127*, 14–26.

Pozzi, D., Lignani, G., Ferrea, E., Contestabile, A., Paonessa, F., D'Alessandro, R., Lippiello, P., Boido, D., Fassio, A., Meldolesi, J., et al. (2013). REST/NRSF-mediated intrinsic homeostasis protects neuronal networks from hyperexcitability. EMBO J. *32*, 2994–3007. https://doi.org/10.1038/emboj.2013.231.

Quadrato, G., and Di Giovanni, S. (2013). Waking up the sleepers: shared transcriptional pathways in axonal regeneration and neurogenesis. Cell. Mol. Life Sci. *70*, 993–1007. https://doi.org/10.1007/s00018-012-1099-x.

Rodenas-Ruano, A., Chávez, A.E., Cossio, M.J., Castillo, P.E., and Zukin, R.S. (2012). REST-dependent epigenetic remodeling promotes the developmental switch in synaptic NMDA receptors. Nat. Neurosci. *15*, 1382–1390.

Samudre, S., Lattanzio, F.A., Jr., Lossen, V., Hosseini, A., Sheppard, J.D., Jr., McKown, R.L., Laurie, G.W., and Williams, P.B. (2011). Lacritin, a novel human tear glycoprotein, promotes sustained basal tearing and is well tolerated. Invest. Ophthalmol. Vis. Sci. *52*, 6265–6270. https://doi.org/10.1167/iovs.10-6220.

Schermer, A., Jester, J.V., Hardy, C., Milano, D., and Sun, T.-T. (1989). Transient synthesis of K6 and K16 keratins in regenerating rabbit corneal epithelium: keratin markers for an alternative pathway of keratinocyte differentiation. Differentiation. *42*, 103–110. https://doi.org/10.1111/j.1432-0436.1989.tb00611.x.

Schneider, C.A., Rasband, W.S., and Eliceiri, K.W. (2012). NIH Image to ImageJ: 25 years of image analysis. Nat. Methods *9*, 671–675. https://doi.org/10.1038/nmeth.2089.

Simsek, C., Kojima, T., Dogru, M., and Tsubota, K. (2018). Alterations of murine subbasal corneal nerves after environmental dry eye stress. Invest. Ophthalmol. Vis. Sci. *59*, 1986–1995. https://doi.org/10.1167/iovs.17-23743.

Singh, S.K., Kagalwala, M.N., Parker-Thornburg, J., Adams, H., and Majumder, S. (2008). REST maintains self-renewal and pluripotency of embryonic stem cells. Nature *453*, 223–227.

Steger, B., Speicher, L., Philipp, W., and Bechrakis, N.E. (2015). In vivo confocal microscopic characterisation of the cornea in chronic graft-versus-host disease related severe dry eye disease. Br. J. Ophthalmol. *99*, 160–165.

Stepp, M.A., Gibson, H.E., Gala, P.H., Drina, D.D., Pajoohesh-Ganji, A., Pal-Ghosh, S., Brown, M., Aquino, C., Schwartz, A.M., Goldberger, O., et al. (2002). Defects in keratinocyte activation during wound healing in the syndecan-1-deficient mouse. J. Cell Sci. https://doi.org/10.1242/jcs.00128.

Su, T., Liu, H., Zhang, D., Xu, G., Liu, J., Evans, S.M., Pan, J., and Cui, S. (2019). LIM homeodomain transcription factor Isl1 affects urethral epithelium differentiation and apoptosis via Shh. Cell Death Dis. *10*, 713–812.

Sugrue, S.P., and Zieske, J.D. (1997). ZO1 in corneal epithelium: association to the zonula occludens and adherens junctions. Exp. Eye Res. *64*, 11–20. https://doi.org/10.1006/exer.1996.0175.

Sun, Y., Dykes, I.M., Liang, X., Eng, S.R., Evans, S.M., and Turner, E.E. (2008). A central role for Islet1 in sensory neuron development linking sensory and spinal gene regulatory programs. Nat. Neurosci. *11*, 1283–1293. https://doi.org/10.1038/nn.2209.

Suvas, S. (2017). Role of substance P neuropeptide in inflammation, wound healing, and tissue homeostasis. J. Immunol. *199*, 1543–1552. https://doi.org/10.4049/jimmunol.1601751.

Szalai, E., Szucs, G., Szamosi, S., Aszalos, Z., Afra, I., and Kemeny-Beke, A. (2021). An in vivo confocal microscopy study of corneal changes in patients with systemic sclerosis. Sci. Rep. *11*, 11111–11117.

Tsai, W.-H. (1985). Moment-preserving thresolding: a new approach. Comput. Vis. Graph Image Process *29*, 377–393.

Ueno, H., Ferrari, G., Hattori, T., Saban, D.R., Katikireddy, K.R., Chauhan, S.K., and Dana, R. (2012). Dependence of corneal stem/progenitor cells on ocular surface innervation. Invest. Ophthalmol. Vis. Sci. *53*, 867–872. https://doi.org/10.1167/iovs.11-8438.

Uusitalo, H., Krootila, K., and Palkama, A. (1989). Calcitonin gene-related peptide (CGRP) immunoreactive sensory nerves in the human and Guinea pig uvea and cornea. Exp. Eye Res. *48*, 467–475.

Vijmasi, T., Chen, F.Y.T., Balasubbu, S., Gallup, M., McKown, R.L., Laurie, G.W., and McNamara, N.A. (2014). Topical administration of lacritin is a novel therapy for aqueous-deficient dry eye disease. Invest. Ophthalmol. Vis. Sci. *55*, 5401–5409. https://doi.org/10.1167/iovs.14-13924.

Villani, E., Galimberti, D., Viola, F., Mapelli, C., Del Papa, N., and Ratiglia, R. (2008). Corneal involvement in rheumatoid arthritis: an in vivo confocal study. Invest. Ophthalmol. Vis. Sci. *49*, 560–564.

Wang, C., Peng, Y., Pan, S., and Li, L. (2014). Effect of insulin-like growth factor-1 on corneal surface ultrastructure and nerve regeneration of rabbit eyes after laser in situ keratomileusis. Neurosci. Lett. *558*, 169–174.

Wang, J., Wang, N., Xie, J., Walton, S.C., McKown, R.L., Raab, R.W., Ma, P., Beck, S.L., Coffman, G.L., Hussaini, I.M., and Laurie, G.W. (2006). Restricted epithelial proliferation by lacritin via PKCα-dependent NFAT and mTOR pathways. J. Cell Biol. *174*, 689–700. https://doi.org/10.1083/jcb.200605140.

Wu, L.-Q., Mou, P., Chen, Z.-Y., Cheng, J.-W., Le, Q.-H., Cai, J.-P., and Wei, R.-L. (2019). Altered corneal nerves in Chinese thyroid-associated ophthalmopathy patients observed by in vivo confocal microscopy. Med. Sci. Monit. *25*, 1024–1031.

Xiao, Y., Thoresen, D.T., Williams, J.S., Wang, C., Perna, J., Petrova, R., and Brownell, I. (2015). Neural Hedgehog signaling maintains stem cell renewal in the sensory touch dome epithelium. Proc. Natl. Acad. Sci. USA *112*, 7195–7200. https://doi.org/10.1073/pnas.1504177112.

Yabuta, C., Oka, T., Kishimoto, Y., Ohtori, A., Yoshimatsu, A., and Azuma, M. (2012). Topical FK962 facilitates axonal regeneration and recovery of corneal sensitivity after flap surgery in rabbits. Am. J. Ophthalmol. *153*, 651–660.e1.

Zhang, Q., Huang, R., Ye, Y., Guo, X., Lu, J., Zhu, F., Gong, X., Zhang, Q., Yan, J., Luo, L., et al. (2018). Temporal requirements for ISL1 in sympathetic neuron proliferation, differentiation, and diversification. Cell Death Dis. *9*, 247. https://doi.org/10.1038/s41419-018-0283-9.

Zhao, H., Feng, J., Seidel, K., Shi, S., Klein, O., Sharpe, P., and Chai, Y. (2014). Secretion of shh by a neurovascular bundle niche supports mesenchymal stem cell homeostasis in the adult mouse incisor. Cell Stem Cell *14*, 160–173. https://doi.org/10.1016/j.stem.2013.12.013.

Zhou, D., Chen, Y.-T., Chen, F., Gallup, M., Vijmasi, T., Bahrami, A.F., Noble, L.B., van Rooijen, N., and McNamara, N.A. (2012). Critical involvement of macrophage infiltration in the development of Sjögren's syndrome–associated dry eye. Am. J. Pathol. *181*, 753–760.

STAR★METHODS

KEY RESOURCES TABLE

REAGENT or RESOURCE	SOURCE	IDENTIFIER
Antibodies		
Mouse anti-ZO1 conjugated to Alex594	Life Technologies	Cat# 339194; RRID:AB_2532188
Rabbit anti-KRT6A	Atlas Antibodies	Cat# HPA061168, RRID:AB_2684440
Chicken anti-KRT14	Biolegend	Cat# 906001, RRID:AB_2565055
Rat anti-Ki67	Biolegend	Cat# 652405; RRID:AB_2561929
Rat anti-CD4	Santa Cruz	Cat# sc-13573; RRID:AB_2108559
Rabbit anti-TUBB3	Cell Signaling	Cat# 5568; RRID:AB_10694505
Rat anti-Ecadherin	Thermo Fisher Scientific	Cat# 131900; RRID:AB_2533005
Mouse anti-TUBB3	R&D Systems	MAB 1195; RRID:AB_357520
Rabbit anti-GAP43	Novus Bio	NB 300-143; RRID:AB_350468
Goat anti-CGRP	Thermo Fisher Scientific	PA1-85250; RRID:AB_2259435
Rat anti-Substance P	Millipore	MAB 356; RRID:AB_94639
Cy^{TM}3 AffiniPure F(ab')$_2$ Fragment donkey anti-Rabbit IgG (H+L)	Jackson ImmunoResearch Laboratory	711-166-152; RRID:AB_2313568
Alexa Fluor 488 AffiniPure F(ab')$_2$ Fragment donkey anti-Rat IgG (H+L)	Jackson ImmunoResearch Laboratory	712-546-153; RRID:AB_2340686
Alexa Fluor 647 AffiniPureF(ab')$_2$ Fragment donkey anti-Chicken IgG (H + L)	Jackson ImmunoResearch Laboratory	703-006-155; RRID:AB_2340347
Alexa Fluor488 AffiniPureF(ab')$_2$ Fragment donkey anti-Goat IgG (H + L)	Jackson ImmunoResearch Laboratory	705-546-147; RRID:AB_2340430
Cy^{TM}3 AffiniPureF(ab')$_2$ fragment donkey anti−Mouse IgG (H + L)	Jackson ImmunoResearch Laboratory	715-166-151; RRID:AB_2340817
Cy^{TM}3 AffiniPure F(ab')$_2$ Fragment donkey anti-Rabbit IgG (H+L)	Jackson ImmunoResearch Laboratory	711-166-152; RRID:AB_2313568
Chemicals, peptides, and recombinant proteins		
Hoechst	Sigma-Aldrich	33342
Mm-Sdc1 RNAscope probe	ACDBio	813921
Lacripep	Dr. Gordon Laurie (University of Virginia)	N/A
Pilocarpine hydrochloride	Sigma-Aldrich	P6503
Critical commercial assays		
RNAscope fluorescent Multiplex Assay v2	ACDBio	323100
RNAqueous^{TM}-Micro Total RNA Isolation Kit	Invitrogen	AM1931
NEBNext® UltraTM RNA Library Prep Kit for Illumina®	New England Biolab inc.	E7530L
PE Cluster Kit cBot-HS	Illumina	PE-401-3001
Deposited data		
RNA Sequencing data	This paper	GEO: GSE208297
Experimental models: Organisms/strains		
Mouse: *Aire*$^{-/-}$/ BalbC	Mark Anderson Lab, UCSF	NA
Software and algorithms		
Image J	(Schneider et al., 2012)	https://imagej.nih.gov/ij/
IMARIS	Oxford Instruments	N/A
GraphPad Prism v8	GraphPad	https://www.graphpad.com
RStudio 2022.02.2	R Studio	https://rstudio.com
Fastp	(Chen et al., 2018b)	https://github.com/OpenGene/fastp

(*Continued on next page*)

Continued

REAGENT or RESOURCE	SOURCE	IDENTIFIER
STAR	(Dobin et al., 2013)	https://github.com/alexdobin/STAR
DEseq2	(Love et al., 2014)	https://github.com/mikelove/DESeq2
Pheatmap	(Kolde, 2015)	https://github.com/raivokolde/pheatmap
DAVID, 2021 update	(Huang et al., 2021)	https://david.ncifcrf.gov/home.jsp
Cytoscape v 3.9.1		https://cytoscape.org
iRegulon	(Janky et al., 2014)	http://iregulon.aertslab.org
EnhancedVolcano	(Blighe et al., 2019)	https://github.com/ke vinblighe/ Enhanced Volcano

RESOURCE AVAILABILITY

Lead contact

Further information and requests for resources and reagents should be directed to and will be fulfilled by the lead contact, Sarah Knox (sarah.knox@ucsf.edu).

Materials availability

This study did not generate new unique reagents.

Data and code availability

- RNA sequencing data have been deposited in the Gene Expression Omnibus (GEO) database with accession code GSE208297, aslisted in the key resources table, and are publicly available as of the date of publication.
- Original microscopy data reported in this paper will be shared by the lead contact upon request.
- This paper does not report original code.
- Any additional information required to reanalyze the data reported in this paper is available from the lead contact upon request.

EXPERIMENTAL MODEL AND SUBJECT DETAILS

Animals

All procedures were approved by the UCSF Institutional Animal Care and Use Committee (IACUC) and adhered to the NIH Guide for the Care and Use of Laboratory Animals (Approval number: 332AN089075-02). Wild type (WT) and *Aire*-deficient mice on the BALB/c background (BALB/c *Aire* KO) were the gift of Mark Anderson, University of California, San Francisco. Adult female mice (aged between 5 and 7 weeks) were used in all experiments. Mice were housed in groups of up to five per cage where possible, in individually ventilated cages (IVCs), with fresh water, regular cleaning, and environmental enrichment. Appropriate sample size was calculated using power calculations. Genomic DNA isolated from tail clippings was genotyped for the *Aire* mutations by PCR with the recommended specific primers and their optimized PCR protocols (Jackson Laboratories Protocol 17936).

METHOD DETAILS

Treatment regimen

Aire KO female mice aged 5 weeks were used for the study. Lyophilized Lacripep was a gift from Dr. Gordon Laurie (University of Virginia) and was reconstituted to a 4 μM solution in PBS. A set of *Aire* KO mice were topically treated with 5 μL per eye of either Lacripep or PBS. Dosing was three times daily for 14 consecutive days. Lissamine green staining assessment and tear secretion assays were performed on each eye before treatment at baseline, 7 days and 14 days post treatment.

Analysis of epithelial barrier function

After mice were anesthetized with isoflurane, 5 μL of lissamine green dye (1%) was applied to the lower conjunctival cul-de-sac. Images of the cornea were then taken using an Olympus Zoom Stereo Microscope (Olympus, CenterValley, PA). Lissamine green staining was scored by dividing the cornea into four quadrants, the extent of staining in each quadrant was classified as Grade 0, no staining; Grade 1, sporadic (<25%); Grade 2, diffuse punctate (25–75%), or Grade 3, coalesced punctate staining (75% or more). The total score was calculated separately for each eye and equaled the sum of all four quadrants ranging from 0 (no staining) to 12 (most severe staining). Scoring was conducted by three masked observers with each data point representing the fold change of each eye relative to its baseline score before treatment.

Tear secretion measurements

Mice were anesthetized with isoflurane and tear secretion was then measured using a Zone-Quick phenol red thread (as indicated by the length of the tear-absorbed region in 15 seconds). To measure physiological tear secretion, mice were first anesthetized with isoflurane, and tear production was measured bilaterally by inserting the Zone-Quick thread to the medial canthus of the mouse eye for 15 seconds per eye. Stimulated tear secretion was measured after 4.5 mg/kg of pilocarpine diluted in saline was injected into the peritoneum (i.p.). Ten minutes later, mice were anesthetized with isoflurane and tear secretion was measured using a Zone-Quick phenol red thread (Showa Yakuhin Kako Co. Ltd., Tokyo, Japan).

Tissue processing and immunohistological analyses

Immunohistological and immunofluorescent analyses of cornea and lacrimal gland samples were performed as previously described (Efraim et al., 2020). Briefly, enucleated eyes were embedded in OCT Tissue Tek freezing media. 7μm and 20 μm sections were prepared from fresh frozen tissues using a cryostat (Leica, Izar, Germany) and mounted on SuperFrost Plus slides. Sections were fixed for 20 min in 4% paraformaldehyde (PFA) at room temperature (RT) and permeabilized using 0.3% Triton X-100 in phosphate buffered saline for 15 min. Sections were then washed in PBS-Tween 20 (PBST) for 10 min, before being blocked with 5% normal donkey serum (Jackson Laboratories, ME) in PBST for 1 hr at RT. After blocking, slides were incubated with primary antibodies diluted in blocking buffer overnight at 4°C. Following 3 washes with PBST, slides were incubated with secondary antibodies diluted in blocking solution at RT for 1 hr.

For immunofluorescent analysis, 7 or 20 μm tissue sections were incubated with the following primary antibodies: mouse anti-ZO1 conjugated to Alexa 594 (1:1000, Life Technologies, Cat 339194), rabbit anti-KRT6A (1:800, Cell Signaling, Cat 4912S), chicken anti-KRT14 (1:1500, Santa Cruz, Cat 515882), rat anti-Ki67 (1:200, Biolegend, 652405), rat anti-CD4 (1:200, Santa Cruz), rabbit anti-TUBB3 (1:500, Cell Signaling, Cat 5568S), and rat anti-Ecadherin (1:300, Life Technologies, Cat 131900). Antibodies were detected using Cy2-, Cy3- or Cy5-conjugated secondary Fab fragment antibodies (Jackson Laboratories), and nuclei were stained with Hoechst 33342 (1:3000, Sigma-Aldrich).

For corneal whole mount staining, PFA fixed corneas were blocked and incubated in primary antibodies for 48hr at 4°C: Mouse anti-TUBB3 (1:300, R&D, MAB 1195), rabbit anti-GAP43 (1:400, Novus bio, NB 300-143), goat anti-CGRP (1:300, Thermo fisher, PA1-85250), and rat anti-Substance P (1:500, Millipore, MAB 356). This was followed by extensive washes in PBST before tissue was incubated in secondary antibodies overnight at 4°C.

Fluorescence was analyzed using a zeiss LSM 900 confocal microscope or Zeiss Yokogawa Spinning disk confocal microscope with images assessed using NIH ImageJ (Schneider et al., 2012) software, as described below.

In situ hybridization

Manual chromogenic RNAscope (ACDBio) was performed using company protocols on fresh frozen cornea tissue sections to detect target RNA at single cell level. Tissue pre-treatment included fixation for 15 min in 4% paraformaldehyde (PFA) at 4°C, RNAscope® Hydrogen Peroxide (ACD# 322335) treatment for 10 min at RT followed by protease treatment (RNAscope® Protease Plus ACD# 322331) for 10 min at 40°C using the HybEZ Oven. Detection of specific probe binding sites was with RNAscope Reagent kit—from ACD (Cat. 323110). Single ISH detection for mouse *Sdc1* (ACD Probe: 813921), Mouse Positive Control Probe (ACD Probe: 320881) and Negative Control Probe (ACD Probe: 320871) was performed manually. Target probes were hybridized for 2 hr at 40°C using HybEZ oven followed by amplification steps according to the manufacture's protocol. Positive staining was indicated by fluorescent dots in the cell cytoplasm or nucleus.

Image analysis

Quantification of tight junction protein ZO1

ZO-1 fluorescent intensity was quantified in the apical squamous epithelial layer within a region of interest (ROI) within the central cornea (350 μm × 350 μm across the corneal epithelium). A Tsai's thresholding method (Tsai, 1985) (Moments) was then applied to the ROI, and integrated densities within the ROI of the thresholded image were recorded.

Quantification of corneal epithelial basal progenitor identity and proliferation

The number of basal KRT14+ and KRT14 + KRT6A + basal epithelial cells were counted in 350 μm sections of central cornea. To obtain the percentage of KRT6A + basal cells per respective region, the number of KRT14 + KRT6A + basal cells was divided by the total number of KRT14 + basal cells. The number of proliferating epithelial progenitors (Ki67 + KRT14+) was presented as a percentage of total KRT14 + cells counted in 350 μm sections of central cornea.

Quantification of CD4+ T cells in cornea and lacrimal gland

The numbers of CD4+ T cells in the limbal stroma were counted and graphed. CD4+ T cells in the lacrimal gland were presented as percent coverage of total CD4+ T cells within the whole lacrimal gland tissue area.

Quantification of corneal epithelial nerve density and synapses

Tissue sections: TUBB3+ nerve density within 300 μm sections of central cornea epithelial ROI was quantified by applying Tsai's thresholding method (Moments), with integrated densities within the ROI of the thresholded image being recorded. Corneal whole mounts: The density of nerve expressing GAP43, SP and CGRP within 354 μm × 396 μm stacked image of the entire epithelium was quantified by applying Tsai's thresholding method (Moments), with integrated densities within the ROI of the thresholded image

being recorded. The density of nerves expressing GAP43, TUBB3, or GAP43 and TUBB3 (% Area of 354 μm × 396 μm, double positive nerve % Area was calculated from colocalization threshold image) was quantified from central cornea images of whole mount cornea and plotted in a stacked bar graph to visualize the proportion of each of the three nerve types. Similarly, numbers of synapses marked by expression of GAP43, TUBB3, or GAP43 and TUBB3 were counted per respective region of central cornea (100 μm^2) and plotted in a stacked bar graph. The density of GAP43 + nerves were quantified from the whole mount cornea images (354 μm × 396 μm) applying Tsai's threshold as described above.

3D reconstruction of nerve fibers

Acquired confocal Z-stacks comprising epithelial and stroma were reconstructed into 3D images using Imaris image analysis software (Bitplane AG, Zurich, Switzerland). The surface of the nuclei (Hoechst) and nerves (TUBB3/GAP43/SP/CGRP) were segmented using the background subtraction threshold. Each channel was obtained separately. Touching nuclei were split by the calculated seed points inside each area.

RNA isolation and RNAseq library generation

Total RNA was collected at 7 days of treatment and purified using RNAaqueous and DNase reagents according to the manufacturer's instructions (Ambion, Houston, TX, USA). RNA quality was assessed using the Agilent 2100 BioAnalyzer, and samples with an RNA integrity $\geq$6.0 were included for RNA sequencing. The synthesis of mRNA libraries was performed by Novogene Corporation Inc. according to their protocols. RNA library was formed by ployA capture (or rRNA removal), RNA fragmentation by covaris or enzyme digestion and reverse transcription of cDNA. Sequencing was performed as described below.

RNAseq analysis

RNA libraries were sequenced on an Illumina NovaSeq 6000 by Novogene Corporation Inc. Depths of 20–30 million 150 bp paired-end reads were generated for each sample. Quality control metrics were performed on raw sequencing reads using fastp (Chen et al., 2018b). In this step, clean data (clean reads) were obtained by removing reads containing adapter and poly-N sequences and reads with low quality from raw data. At the same time, Q20, Q30 and GC content of the clean data were calculated. All the downstream analyses were based on the clean data with high quality. Reference genome and gene model annotation files were downloaded from genome website browser (NCBI/UCSC/Ensembl) directly. Paired-end clean reads were aligned to the reference genome using the Spliced Transcripts Alignment to a Reference (STAR) software (Dobin et al., 2013). DEseq2 was then used to detect differential gene expression between WT, untreated *Aire* KO, PBS treated *Aire* KO and Lacripep treated *Aire* KO corneas based on the normalized count data. Genes were considered differentially expressed if the log2 Fold Change between samples was at least 1, with the adjusted p-value held to 0.05 (Love et al., 2014). Heatmaps and Volcano plot of differentially expressed genes were created using ''pheatmap'', and ''EnhancedVolcano'' R packages, respectively (Blighe et al., 2019; Kolde, 2015).

A list of all significantly modulated genes ($p < 0.05$) was used as input for gene ontology (GO) analysis using the online Database for Annotation, Visualization and Integrated Discovery (DAVID, 2021 update (Huang et al., 2009). We consider an attribute to be significant if its adjusted p value is less than 0.05 relative to an appropriate background gene set.

To identify regulatory networks underlying the impact of Lacripep on tissue regeneration, we used the Cytoscape application *iRegulon* (Janky et al., 2014) to predict master regulators, i.e., transcription factors whose regulons (transcriptional target sets) are highly enriched with the input gene list. A list of all significantly modulated genes ($FC > 1.5$, $p < 0.05$) was used as input and the normalized enrichment score (NES) threshold was set to 3, which corresponds to an FDR of the TF recovery between 3%-9%. Exclusively up-regulated genes for each TF were further used as input for GO analysis using DAVID as indicated above.

QUANTIFICATION AND STATISTICAL ANALYSIS

All data are expressed as mean +SD. A minimum of three independent repeats were conducted in all experiments. Bar graphs were used to summarize the means and standard deviations of each outcome obtained using all data collected from wild type (WT) and *Aire KO* mice. A Student's t-test was used for two group comparisons; a one-way analysis of variance (ANOVA) was used for multiple group comparisons with either Tukey's multiple comparisons test, Dunnett T3, or corrected for multiple comparisons by controlling the False Discovery Rate using Benjamini, Krieger and Yekutieli; $p < 0.05$ was considered statistically significant. A false discovery rate of 0.05 was applied to RNAseq data. A Wald test with Benjamini and Hochberg correction was used for differential gene expression, and a Fisher's exact test was used for Gene Ontology analysis.